

論文 / 著書情報
Article / Book Information

Title	Molecular Dynamics Study of One Component Soft-Core System - Analytical Expression of Non-Equilibrium Relaxation in Constant Pressure Conditions
Authors	Junko Habasaki, Akira Ueda
Citation	Journal of Non-Crystalline Solids, Volume 447, pp. 212-222
Pub. date	2016, 6
DOI	http://dx.doi.org/10.1016/j.jnoncrysol.2016.06.015
Creative Commons	See next page.
Note	This file is author (final) version.

License



Creative Commons: CC BY-NC-ND

**Molecular Dynamics Study of One Component Soft-Core System
-Analytical Expression of Non-Equilibrium Relaxation in Constant
Pressure Conditions**

Junko Habasaki*[†] and Akira Ueda**

** School of Materials and Chemical Technology, Tokyo Institute of Technology,
Nagatsuta 4259, Yokohama 226-8502, Japan*

***Department of Applied Mathematics and Physics, Faculty of Engineering, Kyoto University,
Kyoto 606-8501, Japan*

[†] To whom correspondence should be addressed.

E-mail: habasaki.j.aa@m.titech.ac.jp

Abstract

Analytical expressions of non-equilibrium relaxation for the system with soft-core (SC) potential under the constant pressure condition (using the Andersen method) were derived for the first time and validity of them was confirmed by molecular dynamics (MD) simulations. The path of relaxations can be mapped on the phase-diagram (Compressibility factor g^* plotted against the reduced density ρ^*) using its instantaneous value g_t^* and is found to be a unique function of the reduced density, ρ^* . Contribution of internal energy term to the *NPH* relaxation is found to be about 1/4 of the instantaneous compressibility factor, $g(\rho_t^*)$. It is also shown that different extended conditions resulted in different paths on the phase-diagram. Based on these results, a role of the path and fluctuations on the glass transition is discussed. Further details such as fluctuation of each term of thermal properties and effects of mass of walls are examined to serve a fundamental knowledge of the non-equilibrium relaxation.

Key words Non-equilibrium relaxation, SC model, Molecular Dynamics, Phase-diagram

1. INTRODUCTION

To clarify complex relaxations in supercooled liquids is a long-standing unsolved problem of condensed matter physics and chemistry, which is closely related to the glass transition of the system [1-4]. Although attention tends to be focused on the relaxations in the equilibrated or quasi-equilibrated state, non-equilibrium character of the glass transition should not be forgotten. Previously, non-equilibrium relaxation in *NVE* condition of the system with inverse-power law type potential, $\phi_n(r) = \varepsilon(\sigma/r)^n$, (it is traditionally called as soft-core (SC) model), was examined along the phase-diagram

using the compressibility factor, $\tilde{P}(T^*) \equiv PV / Nk_bT$ ($=g^*$) plotted against the reduced density ρ^* or reduced temperature, T^* . Interestingly, non-equilibrium relaxation can be mapped on the diagram using the instantaneous compressibility factor and it enables us to treat the system, analytically. Although the NVE ensemble is a natural ensemble without modification by walls or thermostat, experiments are usually performed in constant pressure conditions and hence the role of these conditions in the non-equilibrium relaxation is worth to examine.

Our attention is focused on the constant pressure condition by the Andersen method [5], where several walls with different mass are used to control pressure. At first, we derived analytical expressions of non-equilibrium relaxation for the system with inverse power law type potential (SC model, $n=12$) under this condition. To conform the analytical expression, Molecular Dynamics (MD) simulations were performed. Furthermore, details of the thermodynamic variables and the fluctuation of them were examined to serve a fundamental knowledge for understanding the glass transition.

So far, MD simulations have been used to study the dynamics and structures in the systems such as SC model [6-11] and/or Lennard-Jones [12-15] including the problem of the glass transitions. Such works have not only theoretical but also have practical importance. For example, simulations of SC model are successfully compared with experiments of argon and sodium to understand the melting curves [16].

Recently, validity of thermodynamic scaling (*i. e.* the transport coefficient and/or structural α -relaxation time, τ_α , of many glass-formers are/is a function of the product variable, ρ^γ / T , where ρ is the density and T the temperature, where the γ is material constant.) is well established [17-20]. This scaling is frequently argued with the inverse

power law type effective potentials and hence importance of the SC model is increasing. One may consider that the one component system is not suitable for the study of the glass transition because it was known to show a rapid crystallization. Actually, until now, binary systems tend to be used a model of glass transition, since they have stability against the crystallization. One problem of using binary system is that the mixing effect of components is unavoidable [See Ref. 21 and references therein] and this effect may be difficult to separate from other ones.

In earlier works, one component SC system was believed to crystalize easily. However, if the system size is large enough, almost all systems are found to reach the glass branch of the phase-diagram, where the system is in the metastable state rather than to reach the crystal (FCC) branch below it (see Fig. 1(a)). Thus one component system is useful for the study of the glass transition [10,11].

1.1 Effect of Different Extended Conditions on the Glass Transition

In the present work, the system under the constant pressure (*NPH*) conditions was examined, because conventional experimental conditions can be represented by the combination of *NPH* condition and cooling by different rates.

Results obtained by the *NPH* (constant number, constant pressure and constant enthalpy) condition will be compared with those by the *NVE* non-equilibrium relaxation examined in previous works [10,11].

The problem contains two factors; one is difference in the path on the *P-V-T* diagram or on the phase-diagram and another is difference of fluctuations of the systems by the choice of conditions. Treatment of the system under the constant pressure condition in

the theory and/or MD simulations seems to be necessary for further comparison with experiments and deeper understanding of the glass transition.

Some arguments for the effect of different ensembles during the glass transition are found in literatures. For example, Binder [22] has pointed out that it is essential to carry out simulations for examining the glass transition at constant density and not at constant pressure, because in the latter case, there is a too strong dependence of the simulated properties on the cooling rate of the simulation. Although this argument is reasonable in some purpose of the researches, caution is required for the treatment of density during the cooling schedule. If the density is taken from experiments at room temperature and constant volume condition is used throughout the cooling schedule, system is under high pressure at high temperature. In this case, structure under high pressure might result in the high pressure form of the glass. Furthermore, such strong dependency can be a characteristic of the glass transition. For the structure of network, Habasaki and Ngai [23] pointed out that the formation of polymorphs in different Q_n distributions (where n is concerned with the number of bridging oxygen in SiO_4 units.) in the lithium disilicate glass is related to the different path in P - V - T phase-diagram during the cooling or compression schedule used in MD simulation. The resultant network structures of glasses are expected to depend on the history and choice of the conditions.

Of course, different extended conditions also affect the fluctuation of the system.

Recently, Roskilde group [24,25] pointed out that the presence of strong correlations between equilibrium fluctuations of the configurational parts of (instantaneous) pressure and energy for a number of model liquids in NVT ensemble (using the Nosé-Hoover thermostat [26]), and this behavior is argued to be correlated with the validity of the

thermodynamic scaling. Thus the problem of difference of the conditions are non-negligible for the argument of the glass transition. In the present work, it will be shown that the direction of the path and the fluctuation on the phase-diagram are different, if different ensembles are used. This gives a new perspective for understanding glass transition.

2. BACKGROUND

Here we summarize the theoretical formula used for *NVE* condition [8-11].

The Hamiltonian of the SC model is

$$H(p, r) = \sum_j p_j^2 / 2m + \sum_{i < j} \varepsilon (\sigma / r_{ij})^n \equiv K + U, \quad (1)$$

where the m and σ are mass and a size parameter of the particle, respectively.

The Hamiltonian is rewritten as

$$H(p, r) = \varepsilon (\sigma / l)^n H^*(p^*, r^*) \quad (2a)$$

$$H^*(p^*, r^*) = \sum_j p_j^{*2} / 2 + \sum_{i < j} (1 / r_{ij}^*)^n \equiv K^* + U^* \quad (2b)$$

Here the unit system of the length, $l = (V / N)^{1/3}$, time $\tau = l(m / \varepsilon)^{1/2} (l / \sigma)^{n/2}$ is introduced. Values K^* and U^* are the scaled kinetic and potential energies, respectively. According to the classical virial theorem, combined with the *NVE*-MD method, the compressibility factor $PV / Nk_B T$ can be written as

$$\frac{PV}{Nk_B T} = 1 + \frac{n \langle U_t \rangle}{2 \langle K_t \rangle} = 1 + \frac{n \langle U_t^* \rangle}{3 NT^*} \equiv \tilde{P}(\rho^*), \quad (3)$$

where the notation $\langle \dots \rangle$ means the time average. The $\tilde{P}(\rho^*)$ is given by a function of the reduced density ρ^* (or the reduced temperature, T^*) defined by

$$\rho^* = \rho \left(\frac{\varepsilon}{k_B T} \right)^{3/n} = T^{*-3/n}, \quad (4)$$

where $\rho = N\sigma^3/V$ is the non-dimensional number density, and V the volume of the system [6]. On the phase-diagram, where the compressibility, $\tilde{P}(\rho^*)$ is plotted against ρ^* , the glass transition by cooling or compression can be treated on the same basis.

Interestingly, the fluctuation of $\tilde{P}(\rho^*)$ caused by the energy transfer between potential and kinetic energies can be mapped on the diagram [8-11] using a dynamical compressibility factor $(PV/Nk_B T)_t$ defined by

$$\left(\frac{PV}{Nk_B T} \right)_t = 1 + \frac{n U_t}{2 K_t} \equiv g(\rho_t^*). \quad (5)$$

One can represent a path of the non-equilibrium relaxation on the phase-diagram. The following expressions (6a) and (6b) represent a non-equilibrium relation toward the glass branch of the system under the constant energy condition.

$$g(\rho_t^*) = [g(\rho_0^*) + (n/2 - 1)](\rho_t^* / \rho_0^*)^{n/3} - (n/2 - 1) \quad (6a)$$

$$g(\rho_0^*) = (n/3)(E / \varepsilon N)(\rho_0^* / \rho)^{n/3} - (n/2 - 1). \quad (6b)$$

Here $E(= K_t + U_t)$ and $g(\rho_0^*)$ is a given initial value of $g(\rho_t^*)$ with the time dependent reduced density defined by $\rho_t^* = \rho(\varepsilon / k_B T_t)^{3/n}$, and T_t is defined by $k_B T_t = 2K_t / 3N$.

When ρ_t^* fluctuates within the region of thermally equilibrated liquid state (or crystalline state), the longtime averages $\langle \rho_t^* \rangle (\equiv \rho^*)$ and $\langle g(\rho_t^*) \rangle (\equiv \tilde{P}(\rho^*))$ give a point of state on the diagram of $\tilde{P}(\rho^*)$ vs. ρ^* . Behaviors of the quenched glasses as well

as *NVE* non-equilibrium relaxation obey this relation, although in the former system tends to be trapped in the midway of the path toward the glass branch.

Thus *NVE* non-equilibrium relaxations are represented by analytical equations (see (6a) and (6b)). In this case, the non-equilibrium relaxation occurs with fluctuations of reduced density and can be mapped on the phase-diagram by using the instantaneous compressibility factor [9-11]. The *NVE* relaxation is accompanied with the increase of temperature and the decrease of potential energy and hence the process is distinguishable from the equilibrated state easily.

3. MOLECULAR DYNAMICS SIMULATIONS

We study the behaviors of SC system with a pair potential, $\phi_n(r) = \varepsilon(\sigma/r)^n$ ($n=12$) by molecular dynamics simulations using our MD program. MD simulations were performed as in the previous work [10,11,27] using the argon like parameters.

The runs in *NVE* and *NPH* conditions for the system with 2048 particles have been analyzed. Here $H (=E+PV)$ is enthalpy. The time step was set to be either 1 fs or 4 fs (for argon). Cut-off length for the calculation of force was chosen to be 3σ , where the constant temperature is obtained by the scaling of the velocity in each step (it forms a Gaussian thermostat). The system in the liquid state was rapidly cooled ($\sim 1 \times 10^{12}$ K/s for argon) along the liquid branch of the phase-diagram to the initial value of ρ^* to be examined in the supercooled liquid state. The run of more than 200,000 steps was done at each condition for examining non-equilibrium relaxation and run after it was also used for further analyses. The results of time dependence are given using a reduced unit

$$\tau, \text{ where } \tau = l \left(\frac{m}{\varepsilon} \right)^{1/2} \left(\frac{l}{\sigma} \right)^{n/2}.$$

For examining the relaxation process in the constant pressure condition, we used a time development of the value $j(\rho_t^*)$, ($=(\frac{H}{Nk_B T})_t$) denoted j_t^* and dynamical compressibility factor, $g(\rho_t^*)$ denoted g_t^* . Fluctuation of P , g^* and j^* along the non-equilibrium relaxation was examined by MD simulations.

In the present work, several M values were used for each ρ_0^* value under NPH conditions and results are compared with those obtained under the NVE relaxation. For the latter condition, we have done 23 independent runs [10] and confirmed the reproducibility of the path on the phase-diagram and the validity of the equations, (6a) and (6b). For the NPH runs with different mass of walls M ($M=0.0021, 0.021, 0.105, 0.21$ and 2.1) over several orders were compared using a common starting configuration. In the present work, we found that all NPH runs reached to the glass branch on the phase-diagram and similar mass dependences are observed for three different ρ_0^* values ($\rho_0^*=1.4\sim 1.53$). Therefore our attention is focused on the non-equilibrium relaxation starting from $\rho_0^*=1.53$ for the NPH non-equilibrium relaxation. In addition, runs under NPT and NVT conditions were examined to represent the paths and fluctuations depending on the extended conditions.

4. RESULTS

4.1 Derivation of Equations of Non-equilibrium Relaxations in NPH

Condition

At first, we derive the analytical expressions of the non-equilibrium relaxation under the constant pressure condition as follows.

We consider the system containing N particles in the box with the length L (therefore, volume $V=L^3$), where L is determined by the system pressure balancing with the pressure by walls having the mass M (that is, a three dimensional piston) as introduced by Andersen [5].

Hamiltonian in the extended system can be written as follows,

$$H(\mathbf{s}, \boldsymbol{\pi}, V, \Pi) = \sum_i (\boldsymbol{\pi}_i \cdot \boldsymbol{\pi}_i) / (2mV^{2/3}) + U([V^{1/3}\mathbf{s}]) + \frac{1}{2M}\Pi^2 + P_{ex}V \quad (7)$$

, where \mathbf{s} ($=s_{ix}, s_{iy}, s_{iz}$), $\boldsymbol{\pi}_i$ ($=\frac{\partial L}{\partial \dot{s}_i}$) and Π ($=\frac{\partial L}{\partial \dot{V}} = M\dot{V}$) are normalized ($\mathbf{r}_i = L\mathbf{s}_i$)

coordinates, momentum of particle i and momentum of the wall respectively and $P_{ex}V$ is a potential energy by the wall. The system is conservative.

In the equilibrated system with a constant pressure, the term $\frac{1}{2M}\Pi^2$ becomes

negligibly small. If we neglected this term,

$$\langle K + U + P_{ex}V \rangle = \langle E \rangle + P_{ex} \langle V \rangle = const.$$

$$\frac{\langle E \rangle}{Nk_B T} + \frac{P_{ex} \langle V \rangle}{Nk_B T} = j(\rho^*) \quad (8)$$

Here we represent an enthalpy at t as,

$$H_t = E_t + P_{ex}V_t \quad (9)$$

and following relation,

$$\left(\frac{H}{Nk_B T}\right)_t = j(\rho_t^*) \quad (10)$$

is used with $\rho_t^* = \rho_t (\varepsilon / k_B T_t)^{3/n}$.

The subscript t means an instantaneous value.

Eqs. 6(a) and 6(b) explained in Section 2 have been obtained [6,7] based on the classical virial theorem. By the similar procedure to derive these equations, following relation was obtained.

$$j(\rho_t^*) = \frac{E_t}{E_0} \left[\left(\frac{\rho_0}{\rho_t} \right) \left(\frac{\rho_t^*}{\rho_0^*} \right) \right]^{\frac{n}{3}} \left\{ j(\rho_0^*) + \left(\frac{n}{2} - 1 \right) \right\} - \left(\frac{n}{2} - 1 \right) \quad (11)$$

Here, ρ_0^* is an initial reduced density of the system after the quench of the system by temperature scaling, where the non-equilibrium relaxation started in *NPH* condition.

Values E_0 and ρ_0 are the initial internal energy and initial density, respectively.

Derivation of the equation (11) is as follows.

Energy of the system can be written as follows.

$$\left(\frac{E + P_{ex}V}{Nk_B T} \right)_t = \frac{E_t}{Nk_B T_t} + \frac{n}{2} \frac{E_t}{K_t} - \left(\frac{n}{2} - 1 \right) = \frac{E_t}{Nk_B T_t} + \frac{n}{3} \frac{E_t}{Nk_B T_t} - \left(\frac{n}{2} - 1 \right) \quad (12)$$

The relation, $k_B T_t / \varepsilon = (\rho_t / \rho_t^*)^{n/3}$, which was obtained from the $\rho_t^* = \rho_t (\varepsilon / k_B T_t)^{3/n}$, was inserted into above relation,

$$j(\rho_t^*) = \left(\frac{n}{3} + 1 \right) \frac{E_t}{N\varepsilon} \left(\frac{\rho_t^*}{\rho_0} \right)^{\frac{n}{3}} - \left(\frac{n}{2} - 1 \right) . \quad (13)$$

At $t=0$,

$$j(\rho_0^*) = \left(\frac{n}{3} + 1 \right) \frac{E_0}{N\varepsilon} \left(\frac{\rho_0^*}{\rho_0} \right)^{\frac{n}{3}} - \left(\frac{n}{2} - 1 \right) . \quad (14)$$

Therefore,

$$\left(\frac{n}{3} + 1 \right) \frac{E_0}{N\varepsilon} = [j(\rho_0^*) + \left(\frac{n}{2} - 1 \right)] \left(\frac{\rho_0^*}{\rho_0} \right)^{\frac{n}{3}} . \quad (15)$$

Using equations (13) and (15), we obtained the equation (11). This Eq. (11) is an important result of the present work to represent the non-equilibrium relaxation under the constant pressure condition.

The relation,

$$\begin{aligned}
 j(\rho^*) &= h(\rho^*) + g(\rho^*) = \frac{3}{2} + \frac{3}{n}[g(\rho^*) - 1] + g(\rho^*) \\
 &= \left(\frac{3}{2} - \frac{3}{n}\right) + \left(\frac{3}{n} + 1\right)g(\rho^*)
 \end{aligned} \tag{16}$$

is obtained from Eq. (5) and following Eqns. (17) and (18).

Eqns. (17) and (18) are concerned with $h(\rho^*)$ defined by $h(\rho^*) \equiv (E / Nk_B T)$ (see Ref. 27).

$$\frac{E}{N\varepsilon} = t \cdot h(\rho^*), \tag{17}$$

where $t = k_B T / \varepsilon$.

$$h(\rho^*) = \frac{3}{2} + \frac{3}{n}[\tilde{P}(\rho^*) - 1] . \tag{18}$$

If the above relation in Eq. (16) holds during the non-equilibrium relaxation process, the following relation is obtained.

$$g(\rho_t^*) = \left(\frac{3}{n} + 1\right)^{-1} [j(\rho_t^*) - \left(\frac{3}{2} - \frac{3}{n}\right)] . \tag{19}$$

Equations (16) and (19) represent the relation between the $j(\rho_t^*)$ and the instantaneous compressibility factor, $g(\rho_t^*)$. Therefore, using the latter value, non-equilibrium

relaxation under the constant pressure condition can be mapped on the phase-diagram.

From these relations, values of $j(\rho_t^*)$ is found to be about 5/4 of $g(\rho_t^*)$ when $n=12$, if

we neglected the constant term. Therefore, contribution of internal energy term in the non-equilibrium relaxation is about 1/4 of instantaneous compressibility factor, $g(\rho_t^*)$.

In the rest of this subsection, the pressure and mass of walls used to control the constant pressure conditions related to above derivations will be explained.

The system under the constant pressure condition is controlled by the difference of external pressure and internal pressure. The inner pressure P is given by the following form.

$$P = \frac{\varepsilon}{\sigma^3} \left(\frac{k_B T}{\varepsilon} \right)^{3/n+1} \rho^* \tilde{P}(\rho^*) \quad (20)$$

Here the compressibility factor introduced in Ref. 6, $\tilde{P}_n(\rho^*)$ and ours is related by the equation $\tilde{P}(\rho^*) = \tilde{P}_n(\rho^*) / \rho^*$.

Comparing the dimension between mass of the wall and the particle, we see that M has a dimension, $[\text{mass}][(\text{length})^{-4}]$. Then we use the reduced mass M' which is given by the following relations [28],

$$M' = M\sigma^4/m. \quad (21)$$

Hereafter M' is written as M .

4.2 Phase-Diagram of the SC System and *NPH* Relaxation Shown on the Diagram

MD simulations are used to check the expressions mentioned in the section 4.1 and to examine further details of the non-equilibrium relaxation.

In Fig. 1(a), the phase-diagram of the system including the glass branch examined in previous works [10,11] is shown. In *NVE* conditions, the system on the liquid branch is

unstable above $\rho_0^* \sim 1.3$ and it initiates a non-equilibrium relaxation process toward the glass branch [10].

Here the glass branch is defined by the curve connecting metastable positions after the

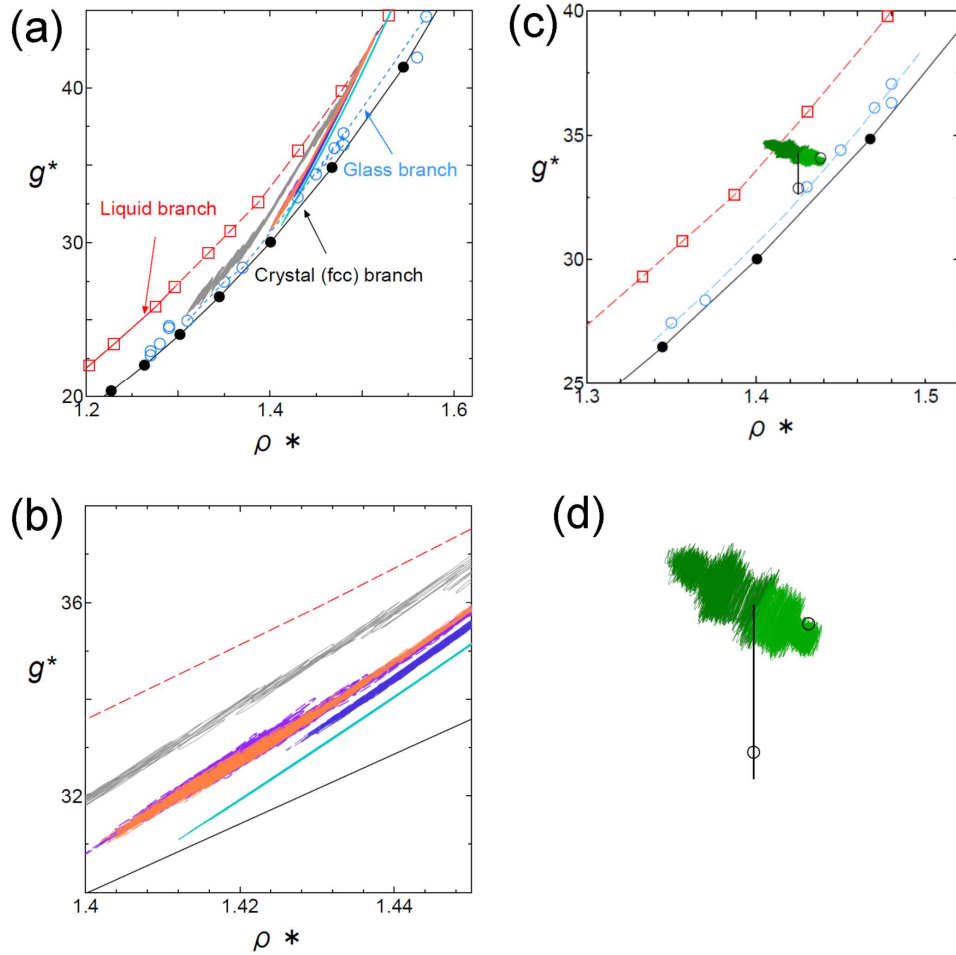


Fig. 1(a) (Color online) (a) Phase-diagram and non-equilibrium relaxations in NPH condition represented by g_t^* . Open squares (red) are g^* for liquids (connected by a solid (red) curve) and super cooled liquids (connected by a dashed (red) curve), while filled circles (black) are for FCC crystal (connected by a solid (black) curve). Open circles (blue) are metastable positions after the NVE relaxation obtained in Ref. 10. The curve connecting the positions is defined as the glass branch. The value g_t^* is related to j_t^* by Eq. (19) in the NPH condition. Four curves were started from the same configuration at $\rho_0^* = 1.53$ with several different mass of the wall (blue: $M=0.0021$, purple: $M=0.021$ orange: $M=0.21$ and gray: $M=2.1$) (from right to left). A thin curve (pale blue) is NVE relaxation started from the slightly larger ρ_0^* . (b) Curves in (a) are shown in an enlarged scale. Except for the heaviest wall (gray: $M=2.1$) case, all curves starting from the same structure in NPH conditions are only slightly different on the phase-diagram. (c) Comparison of the paths for NPT and NVT relaxations on the phase-diagram. The curve for NPT (Green) (during $t/\tau=3 \times 10^4$) started from $\rho_0^* = 1.42$ are followed by the NVT (Black) relaxation and additional NPT runs (Bright green). The NVT relaxation looks like a straight line, while NPT relaxation curves developed from left to right with large fluctuations. The path and its fluctuation for the NVT relaxation are fairly different from those in NPT runs. The final positions after the run of $t/\tau=3 \times 10^4$ are marked by open black circles for both cases. (d) The NPT and NVT runs in (c) are shown in an enlarged scale.

non-equilibrium relaxations, on which the system is considered as a stabilized glass after aging. The position of crystal branch (FCC) is obviously below and separate from this branch on the phase-diagram. Both equilibrated and non-equilibrated values of the compressibility factor were represented as g^* . Similar non-equilibrium relaxations are found in *NPH* runs. Actually, all *NPH* runs (for $\rho_0^*=1.4\sim 1.53$) show non-equilibrium relaxations and reached to the glass branch (slightly above the glass branch obtained by *NVE* runs). In Fig. 1(a), *NPH* runs starting from $\rho_0^*=1.53$ with several M values are plotted. For the comparison, *NVE* relaxation started from the nearby ρ_0^* value on the diagram is shown. Curvatures found in the *NPH* relaxation are slightly different from that in the *NVE* relaxation and final positions after the relaxations have lower ρ^* and larger g^* values. In this figure, non-equilibrium *NPH* relaxation curve for $M=2.1$ (gray) was found to deviate from other curves considerably, while the curvature for the smallest M in *NPH* conditions is comparable to the case of *NVE* relaxation. Other curves are comparable each other, but are slightly modified by the different mass. If *NPH* non-equilibrium relaxation moves along a unique path in the $j(\rho^*) - \rho^*$ plane, it will also hold in the $g(\rho^*) - \rho^*$ diagram from Eq. (19) and this can be judged from the plot.

Difference of the fluctuations by different conditions can be also shown in this figure. Curves for *NPH* relaxations are found to have larger width due to fine structures of the fluctuation. To see it clearly, they are shown in an enlarged scale in Fig. 1(b).

4.3 Comparisons of Non-Equilibrium Relaxations in Different Extended Condition

In Figs. 1(c) and 1(d), relaxation curves for NPT and NVT conditions are shown. The latter relaxation started from the same configurations obtained from the initial stage of NPT relaxation (See caption of Fig. 1(c) for details). In this plot, NVT relaxation looks like a straight line, while the NPT relaxation looks like a ball of yarn due to the large fluctuation.

If we compared the constant volume and constant pressure conditions in Figs. 1(c) and 1(d), it is found that the path of each run shows different direction on the phase-diagram. Due to the temperature control, increases of the temperature observed in NVE and NPH conditions are suppressed by removal of heat from the system and the g^* decreases more directly toward the glass branch.

When different value of M is used, the fluctuations of the systems are modified considerably. In Fig. 2, fluctuations of P' (=inner pressure/external pressure) of the system for four different M values (The fluctuation with $M=0.105$ is comparable to that for $M=0.021$ and is not shown) and fluctuation of H' ($=H/H_0$) during the corresponding runs are shown, where the same initial configuration as in Fig. 1(a) and (b) was used.

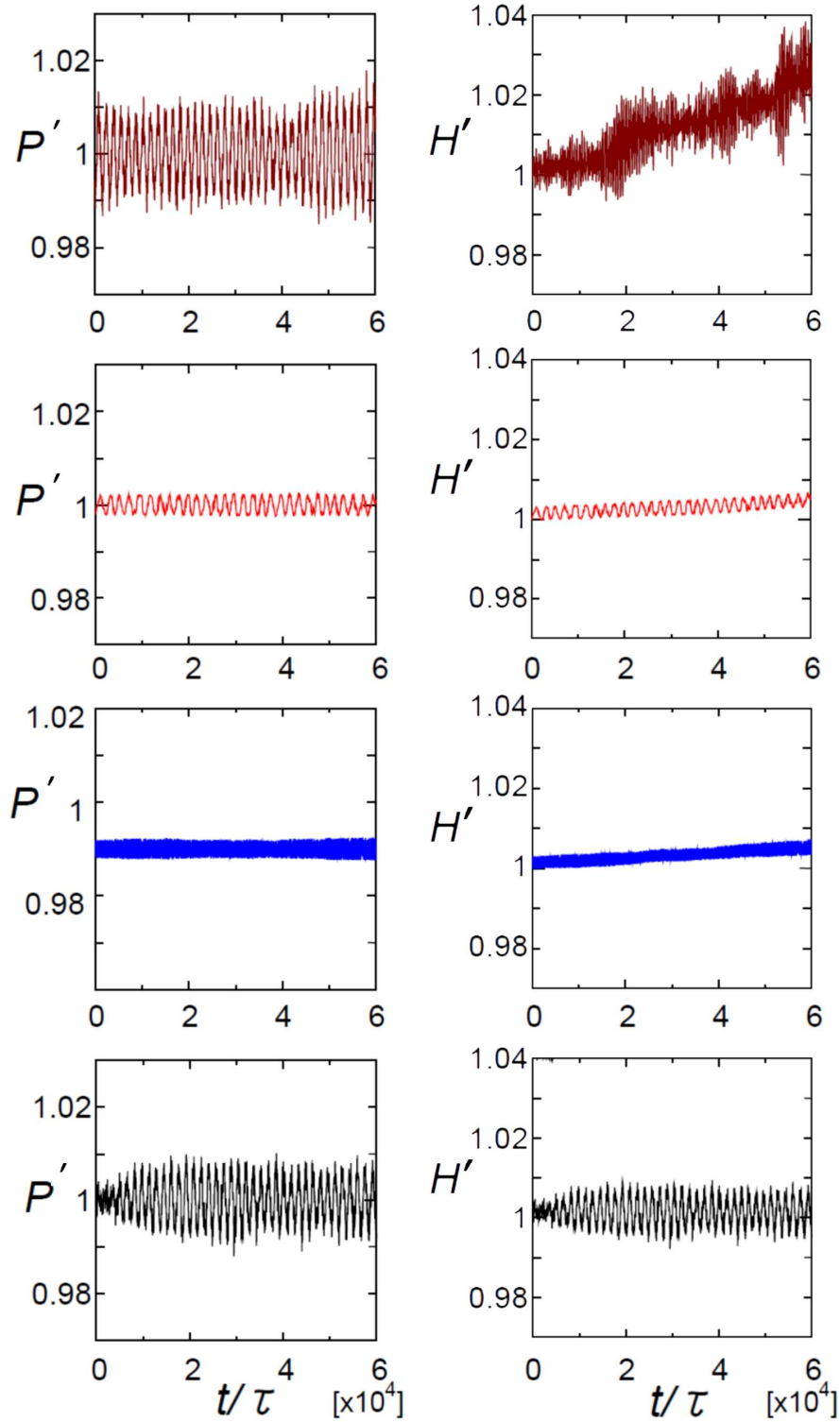


Fig. 2 (Color online) (Left panel) Fluctuations of the relative pressure P' (inner pressure divided by the external pressure being set in advance) and (Right panel) H' ($=H/H_0$), during the *NPH* relaxation ($\rho_0^*=1.53$) in several systems with different mass of walls in the Andersen method. The mass of the wall is $M=2.1$ (brown), $M=0.21$ (red) $M=0.021$ (blue) and $M=0.0021$ (black), from top to bottom for each case.

The largest fluctuation of P' is found in the case of the largest M ($=2.1$). Corresponding H' shifted considerably during the run and therefore this condition is not suitable for the NPH condition. With the largest M , temperature and system volume is found to increase rapidly, while mean pressure is nearly kept constant. It means that the kinetic energy of the wall is non-negligible and particles are affected by it.

Here we note that NPH condition does not necessarily mean the NPH ensemble. In the middle region $0.021 \leq M \leq 0.21$, a pressure control works well with a small drift of H' (within 0.5% during the run). Although the H is a conservative amount in the NPH ensemble in the equilibrated system, it is not necessarily conserved in the non-equilibrium condition or for slow dynamics observed in the limited time scale, while the control of the pressure is successfully done within the observation time. Similar discussion holds for other conditions and therefore, it is better to distinguish terminologies of “condition” and “ensemble”.

In these cases, fluctuation of P and V is found to be antiphase (Details are shown in Fig. 6) and therefore, the pressure control of the system works well. When M is heavier, the frequency of the fluctuation becomes smaller. A width of the fluctuation becomes large when it is comparable to the natural frequency of the system. For the smallest M ($=0.0021$), beat was found and it suggests the P and V in the system is not an exact antiphase here.

To examine the validity of expressions derived in the present work, Eq. (11) is compared with Eq. (16). For several NPH non-equilibrium relaxations, we have confirmed that $j_i(\rho^*)$ plotted against time obtained from Eq. (11) and that by Eq. (16)

completely overlapped. For example, plot of the latter against the former shows the slope of 0.9992 for the $M=0.021$ and this result is shown in Fig. 3.

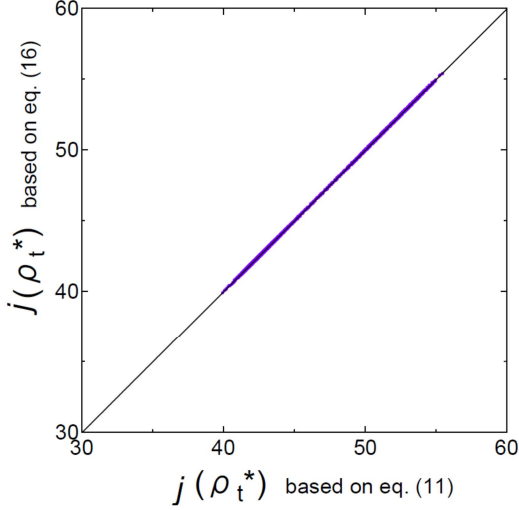


Fig. 3 (Color online) The $j(\rho_t^*)$ values obtained by Eq. (11) is compared with those obtained by Eq. (16).

In this case, 2000 data points are included in the plot and every instance during the *NPH* relaxation, Eq. (11) is comparable to Eq. (16).

In Fig. 4, g_t^* values are plotted against time for $M=0.0021, 0.021$ and 0.21 . A result of *NVE* non-equilibrium relaxation starting from the slightly larger ρ_{0^*} is also shown for the sake of comparison.

The shapes of the relaxation curves in Fig. 4 (a) are compared. The inflection in the relaxation curve is clearer when the heavier wall was used. Black curves are reconstructed ones obtained by a few numbers of principal components using the singular spectrum analysis (SSA) [29]. In Fig. 4(b), a kind of phase-space plots [30] of such relaxations, where $dg^* (=g^*_t - g^*_{t-dt})$, where dt corresponds to 100 steps) is plotted against g^* , are shown using the reconstructed (de-noised) data.

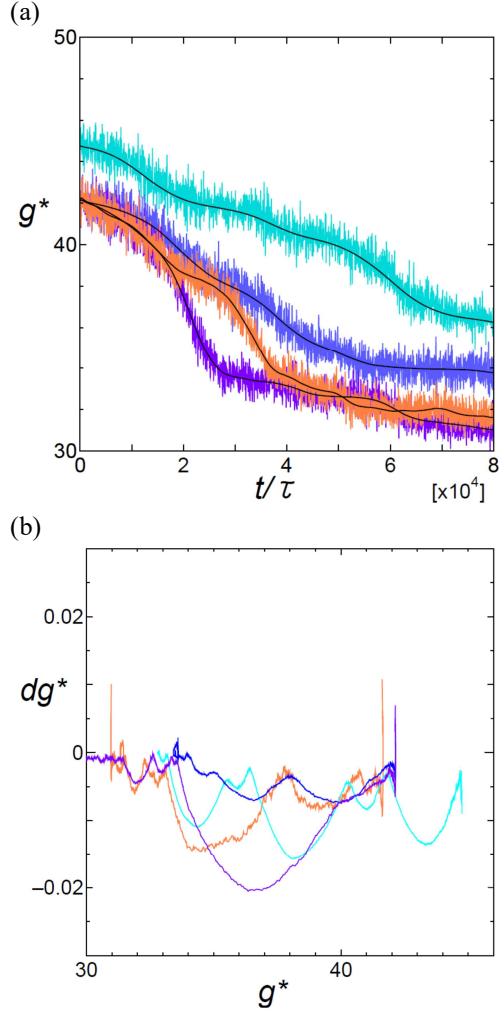


Fig. 4 (Color online) Three curves for g_t^* in *NPH* conditions ($\rho_0^*=1.53$) are shown as a function of time. The values of mass of the wall used are $M=0.0021$ (blue), 0.021 (purple) and 0.21 (orange), respectively. The g_t^* is connected to j_t^* by Eq. (19). Pale blue curve is for the *NVE* relaxation starting from a slightly larger ρ_0 value. (b) Phase-space plots of the developments of the *NVE* and *NPH* relaxations using the de-noised data. De-noising has been done by the singular spectrum analysis (SSA), which is a principal component analysis of the time series. Clear structures (formed by parts of the oval) are found in each curve meaning the deterministic nature of the development. In the beginning of the curves (They started from the right), large changes in g^* are found. In *NPH* conditions, the structure with a longer wave length is found when the mass of wall is heavier. Small fluctuations also overlap to curves.

Previously, a similar plot ($d|\mathbf{r}|=|\mathbf{r}_t-\mathbf{r}_{t-dt}|$ is plotted against $|\mathbf{r}|$, where the \mathbf{r} is displacement vector of ion) has been successfully used to characterize the ionic motion in lithium silicate [31] and ionic liquids [32]. In a similar manner, deterministic character of the “thermodynamical” change of the system is visualized by the plot. These plots start

from the right side and move to the left side with the relaxation. In this kind of plot, clear structure is found if the change is deterministic and oval shapes are found if the change is vibrational. Actually, a clear structure with parts of the oval is found in the *NVE* relaxation, while a structure with some small bumps is found in the case of *NPH* condition. They seem to modify the oval like structures to more hindered ones. Thus the shape of the relaxation curve found in g^* is characterized by the deterministic structure but is affected by the fluctuation of the system.

4.4 Comparison of the Non-equilibrium Relaxation in *NVE* Condition and *NPH* condition

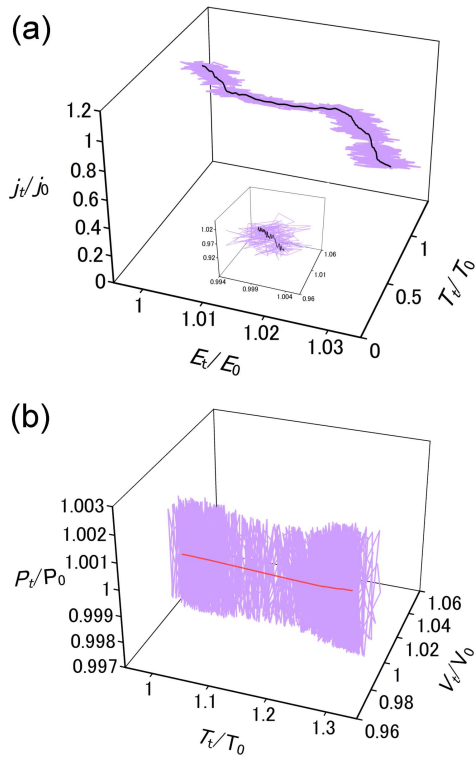


Fig. 5 (Color online) (a) Time dependence of j_t/j_0 for the *NPH* non-equilibrated relaxation is shown as a function of E_v/E_0 and T_v/T_0 for the run with $M=0.021$ shown in Fig. 4. (a) The j_t fluctuates with both values as predicted by Eq. (11).

(b) Fluctuations of relative pressure (P_v/P_0) plotted against that of relative volume (V_v/V_0) and relative temperature (T_v/T_0) during the same run shown in (a).

Fluctuations of the systems also depend on the conditions used. Some details for fluctuations of variables in *NVE* and *NPH* conditions will be shown here. In the *NPH* run, the fluctuation of $j_t (= j(\rho_t^*))$ is caused by those of both E_t and T_t . This is predicted by Eq. (11) and this situation is shown in Fig. 5(a) for the case with $\rho_0^* = 1.53$ and $M=0.021$. A curve after the smoothing by the local polynomial fitting is shown in black. Inset shows the fluctuation for the beginning of the same run in an enlarged scale. In Fig. 5(b), fluctuation of the pressure (P_t/P_0) for this case is shown as a function of T_t and V_t . The curve after the smoothing is shown in red.

In Figs. 6(a) ~ (d), time dependences of some thermodynamic terms are compared. Here, data are normalized by using the initial values.

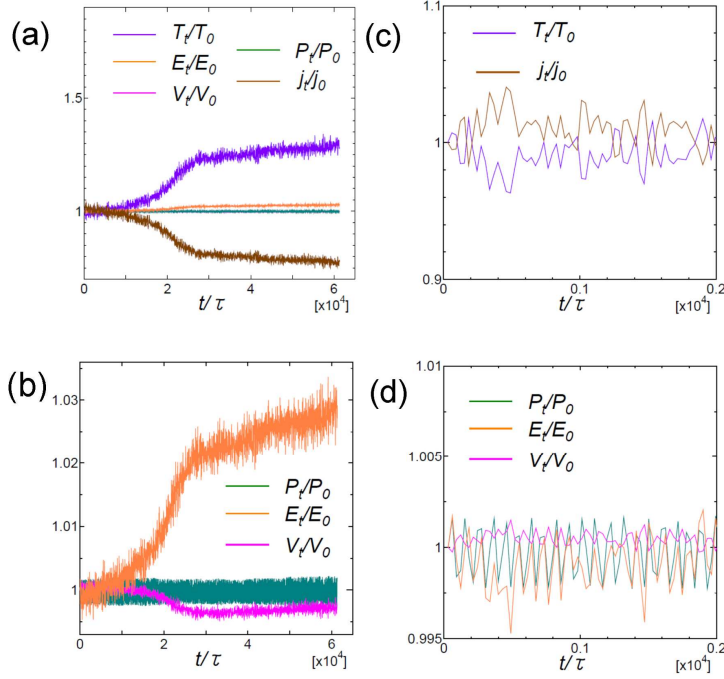


Fig. 6 (Color online) (a) Time dependence of the fluctuations of variables during the *NPH* run with $M=0.021$. Curves are T_v/T_0 , E_v/E_0 , P_v/P_0 and j_v/j_0 from top to bottom. The fluctuation of T_v/T_0 and j_v/j_0 are larger than other variables. Increase in the former and decrease in the latter are dominant process for the *NPH* non-equilibrium relaxation. The curve for V_v/V_0 is hidden by other curves and therefore it is shown in an enlarged scale in (b). (b) The same curves in (a) for P_v/P_0 , E_v/E_0 and V_v/V_0 (bottom in the right part) are shown in an enlarged vertical scale. (c) The plot for a beginning of the same run in an enlarged scale for T_v/T_0 (lower curve) and j_v/j_0 (upper curve). (d) The plot for a beginning of the same run in an enlarged scale for P_v/P_0 , E_v/E_0 and V_v/V_0 . The smallest fluctuation is found for V_v/V_0 .

As shown in Fig. 6(d), relative pressure and volume show antiphase fluctuations. In the case of equilibrated condition [28], this situation is known to occur when the mass of the wall is relatively small.

4.5 Structures Obtained after *NPH* Relaxations

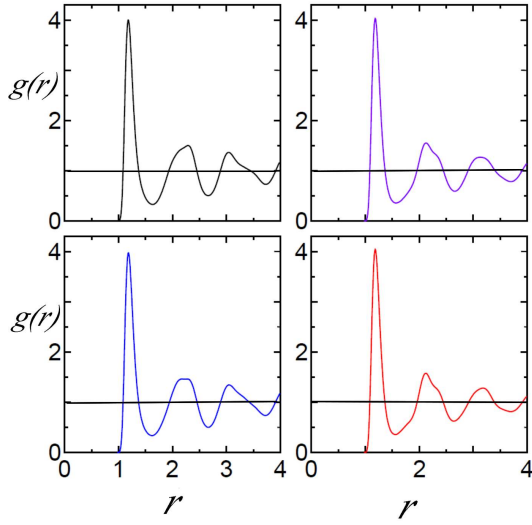


Fig. 7 (Color online) Pair correlation functions $g(r)$, obtained during *NPH* relaxations with different mass of wall. Left panel: top: $M=0.0021$ (black), bottom: $M=0.021$ (blue); Right panel, top: $M=0.105$ (purple), bottom: $M=0.21$ (red).

Structures found after the *NPH* non-equilibrium relaxations (starting from $\rho_0^*=1.53$) using different mass of walls are compared in Fig. 7. In all of these figures, the splitting of the peaks is not clear and structures are different from crystals. From the characteristics of $g(r)$, all samples can be judged in the glassy state. This is because the $g(r)$ function is different from that of FCC and BCC and it lacks the long ranged correlations [10], although an overlap of crystallization process is not excluded here. Some differences were observed if we compared the structures obtained with different M values. We note that both $g(r)$ and $n(r)$ systematically changed with the value of M .

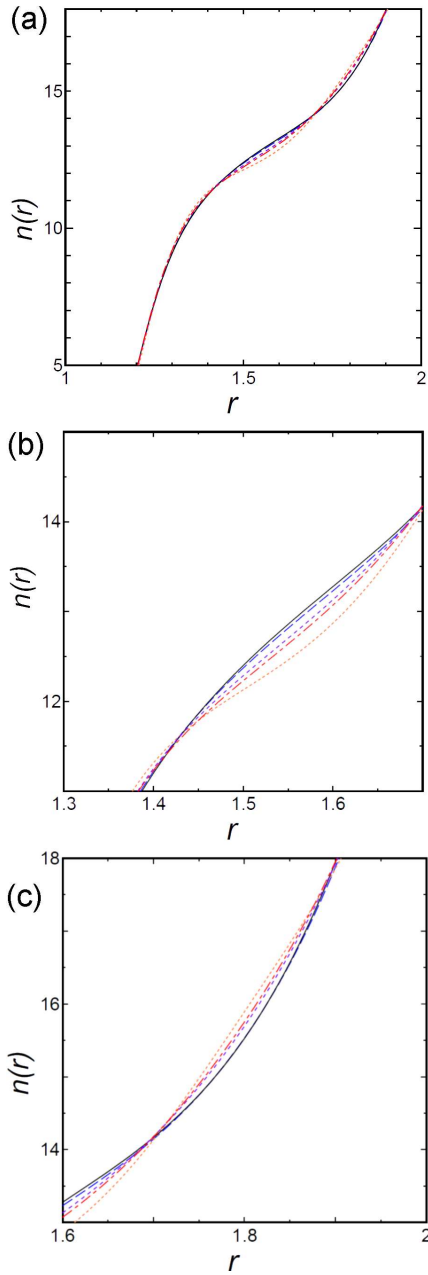


Fig. 8 (Color online) (a) Running coordination functions $n(r)$, obtained after the *NPH* relaxation shown in Fig. 1 with different mass of wall. $M=0.0021$ (black, solid), $M=0.021$ (blue,dashed), $M=0.105$ (purple, short dashed), $M=0.21$ (red, dot dashed), $M=2.1$ (orange, dotted). (b) The same function shown in an enlarged scale. Systematic changes of the function with M is clearly found for the first coordination shell. (c) The same function shown in an enlarged scale for the second coordination shell.

As shown in Fig. 7, positions and heights of first peaks in $g(r)$ for different M values are only slightly different. The shape of the second peaks for larger M values (0.105 and 0.21) is slightly sharper and hindered than that for smaller M values (0.0021 and

0.0021). Corresponding change is observed in the running coordination number $n(r)$ shown in Fig. 8 (a). The contribution at around $r=1.5$ decreases with increasing M and opposite trend is found at around $r=1.8$ and this trend is clearer in Figs. 8(b) and 8(c) shown in an enlarged scale. Namely, the decrease of the coordination number with increasing M in the first coordination shell is compensated by the increase of it in the longer length structure.

5. DISCUSSION

5.1 Difference of the Non-Equilibrium Relaxations in the Different Extended

Condition

From Fig. 1, we have shown that the different extended ensemble resulted in the different path in the phase-diagram and the path of the NPH relation shows a slightly different slope from that for NVE relaxation. The largest deviation of the curve of the NPH relaxation from NVE relaxation is found for the system with the largest mass of the wall and it is probable that some correlated structures are destroyed by the motion of the wall.

The small difference of the curves in NVE and NPH conditions in the non-equilibrium relaxations is not a self-evident thing. This fact becomes clear if we compare the NPT relaxation and NVT relaxation on the same diagram. A different direction of the paths is found in Figs. 1(c) and 1(d). The large effect of the temperature control found in these figures is natural, because the increase of system temperature is found in the constant energy conditions and the heat of the system is taken away by the temperature control.

One can also find that not only the path on the phase-diagram but also the fluctuation of it depend on the extended conditions of MD simulations, considerably. The fluctuation of the curve is not determined by that of ρ^* only, although the position on the phase-diagram is essentially determined by it.

5.2 Validity of Analytical Expressions

For expression of 6(a) and 6(b) for *NVE* relaxation, one can estimate the behavior of the system by changing ρ_t^* . On the other hand, for expressions of Eq. (11) for *NPH* condition, direct mapping is difficult because the $j(\rho_t^*)$ is a function of both E and ρ . Therefore we confirmed the validity of expressions by several steps.

At first, we mapped $g(\rho_t^*)$ on the phase-diagram to check if the $j(\rho^*)$ shows a unique path during the *NPH* relaxation irrespective of different conditions such as choice of M .

If the *NPH* non-equilibrium relaxation moves along a unique path in the $j(\rho^*) - \rho^*$ plane, we can expect it also holds in the $g(\rho^*) - \rho^*$ diagram from Eq. (19). In fact this is the case observed in Fig. 1(a), and each path on the phase-diagram is found to be a unique function of ρ^* for the medium M value cases. Results with different mass of walls can be used not only to choose the suitable M , but also to learn the effect of different fluctuations on the non-equilibrium process. Fluctuations of thermodynamic variables are examined in Fig.2 to see the effect of different M values using the relative pressure P' (inner pressure divided by the external pressure being set in advance) and H' ($=H/H_0$), during the *NPH* relaxation. From Fig. 2, it is found that the condition of the largest M is no more suitable to keep the constant pressure conditions. Therefore, this

case can be excluded in this argument of the validity of the expressions. For other cases, the relaxation shows the unique path on the phase-diagram.

In the next step, we confirmed that the relation between equations (11) and (16), where the instantaneous enthalpy during the relaxations was calculated by the different routes.

As shown in Fig. 3, the relation of $j(\rho^*)$ obtained by Eq. (11) is completely overlapped to that obtained by Eq. (16). The non-equilibrium relaxation with $M=0.021$ shows the large change of g_t^* value during the run as shown in Fig. 4(a). It is interesting to note that even in this case, the relation between Eqns. (11) and (16) holds well. From these results, assumptions used to derive (11) and (16) seem to be reasonable.

Further characteristics such as the relation among several thermodynamic variables are also consistent to the expressions.

5.3 Deterministic Character of the Relaxations

From Fig. 4(a), the shape of the relaxation curves seems to be different case by case, while the positions in the phase-diagram are comparable if we started the same ρ_0^* . Such differences in the shape of the relaxation curves were found previously even in *NVE* runs without modification by walls [10], where 23 independent runs in several conditions including larger system size and longer runs had been examined.

In the present work, a kind of phase-space plots is used to show the deterministic nature of the “thermodynamic” variable, for the first time. The cause of the fluctuations of the relaxation pattern can be explained by the deterministic character of them as discussed below. Such characteristics are shown by the phase-space plot (dg^* plotted

against g^*) in Fig. 4(b). Clear structures representing deterministic nature of the relaxations are found and the spike like changes in dg^* are also found for the beginning of the non-equilibrium relaxations. The results for *NPH* relaxations have more bumps compared with *NVE* relaxation and modification of the shapes is found in the formers. This suggests that the large fluctuation affect the details of the relaxations. That's why the shape and timing of the start of the relaxation changes case by case.

One may consider that the relaxation curves should be treated with better statistics. However, extremely large number of runs is required to take an average of such decay curves, due to the deterministic character and discontinuous events concerned it. In the present work, averaging these relaxation patterns is out of focus, because reproducibility of the paths on the phase-diagram is already good and this is our target of debate.

5.4 Fluctuation Found in the Non-Equilibrium Relaxation

In the case of *NVE* conditions, the dynamical compressibility factor changes with time along the $g(\rho_t^*)$ curve, accompanying the fluctuation of ρ_t^* as shown in the equations 6(a) and 6(b). If an initial point $(g(\rho_0^*), \rho_0^*)$ is located in the region of unstable state, the system relaxes, fluctuating together with ρ_t^* . In the case of constant pressure conditions, $j(\rho_t^*)$ fluctuate instead of $g(\rho_t^*)$ and total energy of the system fluctuates as well. In both *NVE* and *NPH* relaxations, U^* decreases to compensating increase of ρ^* . In the *NPH* run, the fluctuation of $j_t (= j(\rho_t^*))$ is caused by that of E_t and T_t as represented in Eq. (11) and this situation is shown in Fig. 5(a) for the case with $\rho_0^* = 1.53$ and $M=0.021$.

In Fig. 5(b), fluctuation of the pressure (P/P_0) for this case is shown as a function of T_t and V_t . The curve after the smoothing is shown in red.

Since details for the fluctuation of thermodynamics in the non-equilibrated relaxation are unknown, fundamental relations among variables are examined and shown in Fig. 6(a) ~ (d). These results at every instance during the runs are consistent to the analytical representation obtained in the present work.

5.5 Structures obtained after the *NPH* Non-Equilibrium Relaxations

Obtained structures after *NPH* relaxation are quite similar to those obtained near the glass branch in *NVE* relaxations [10,11] as shown in Fig. 7 and 8(a). The $g(r)$ shows some characteristics of glasses different from BCC nor FCC structures. The lack of the clear plateaus in the running coordination number, $n(r)$ in Fig. 8 also means the system is not in the crystalline state. With increasing M , the contribution at around $r=1.5$ decreases and opposite trend is found at around $r=1.8$.

As a whole, coordination shells are slightly clearer when the M is smaller.

It means that a partial crystallization or development of the local packing occurs when M is smaller. The present results reveal that the packing of the structures is affected by the fluctuation of the system during the non-equilibrated relaxation and hence it is related to the formation of glasses.

The fluctuation of the system by the wall affects the local packing of the system and its compressibility. How is the change of the packing related to the glass transition?

Recently, Habasaki and Ngai have reported [33] that the number of constraints of the system and the geometrical degree of the freedom of the coordination polyhedra play roles in the fragile behavior of the glass transition for a typical ionic liquid, 1-ethyl-3-

methyl imidazolium nitrate (EMIM-NO₃). The packing of the coordination polyhedra as well as rigidity percolation of fictive bonds (contact ion pairs) takes important roles there. The role of the packing in the system is to be taken into account for the glass transition of the system.

5.6 Relations with the Problem of the Glass Transition

5.6.1 Definition of the Glass Transition

In the previous works [10,11], glass transition is defined by the positions on the phase-diagram as follows. When the liquid is rapidly cooled ($\sim 1 \times 10^{12}$ K/s for argon) along the liquid branch of the diagram, the system can be supercooled and the glass transition occurs. Structures thus obtained are liquid like (but has more closed packing locally) when it is near the liquid branch. This corresponds to the usual definition of the glass by the procedure how to obtain it. We called this type of glass as a quenched glass. In the region near $\rho_0^* \cong 1.36$, a non-equilibrium relaxation starts after some leading times, while in the region larger than $\rho_0^* \cong 1.4$, a non-equilibrium relaxation immediately started in *NVE* conditions. In our previous study [10], it was shown that most of runs of *NVE* relaxations in the one component SC system ($N=2048, 2067, 4096$) resulted in the metastable states and they are judged to be in the glassy state from both structures [10] and thermodynamic properties [11]. Even for the rapidly quenched system, non-equilibrated relaxation starts at $\rho_0^* = 1.4$. Both states trapped one and metastable states on the glass branch, are considered as the glassy states. This is because the quenched glass also shows the relaxation toward the glass branch (aging), after long time relaxation time. In other words, the quenched glass is considered as in a trapped state on

the way to the glass branch [10] and there are no differences in the characteristics of the relaxation processes observed in both cases. The difference found is mainly for the location on the phase-diagram. A rapidly quenched system tends to be trapped on the midway toward the glass branch for long time. Therefore the quenched system can be located near the liquid branch, while the glass branch is located near the crystal (FCC) branch. Using this definition one can understand the cooling rate dependence of the glass transition, aging and structural changes during the relaxation processes. If the system was rapidly cooled, the system will be located near the liquid branch of the phase-diagram, while the system is cooled more slowly, the non-equilibrium relaxation will start at smaller ρ_0^* value and it will proceed during the cooling. Naturally, similar discussion holds for the case of constant pressure conditions, although the actual paths and fluctuations on the phase-diagram are different. If a rapid cooling rate is used, the system shows the path near the liquid branch of the phase-diagram, while if a slower cooling rate is used, the path would be nearer to the relaxation path for the *NPH* or *NPT* condition. Usually, studies of the glass transition in experiments are performed under constant pressure condition combined with the different cooling rates. Therefore, thermodynamics examined under the constant pressure condition in the supercooled liquids are useful to consider the problem of the glass transition.

The above definition of the glass transition discussed in previous works [10,11] may not necessarily be the same as those by other researchers. Actually, the definition of the glass transition tends to be different by researchers.

One should note that if one used different definition of glasses or the glass transition, it may affect the understanding of the glasses or glass transition; however, it does not

affect the main results of the present work. That is, they are concerned with expressions of non-equilibrium relaxations and related results of MD simulations.

5.6.2 Relation between Thermodynamic Scaling and Glass Transition

As mentioned in Introduction, the thermodynamic scaling of glass forming systems has been well established in many systems. Namely, the structural α -relaxation time, τ_α , or other transport properties of small molecular and polymeric glass-formers obey thermodynamic scaling. In the SC system, thermodynamic scaling holds exactly [6,11,34,35] and hence scaling behavior suggests the existence of effective inverse-power law type potentials in many materials. Concerned with this scaling behavior, fluctuation of the thermodynamic variables may be considered to play important roles in the glass transition. For example, by the Roskilde group [24,25], the presence of strong correlations between equilibrium fluctuations of the configurational parts of (instantaneous) pressure and energy for a number of model liquids in NVT ensemble has been shown by MD. An effective inverse law type potential dominating fluctuations (in the equilibrium system) is argued to be responsible for the thermodynamic scaling, based on the pressure-energy correlations. In general, details of the fluctuation of thermodynamic properties depend on the thermodynamic condition used [36], while the thermodynamic scaling holds regardless the conditions in the SC model in the equilibrated system. However, for some dynamical quantities determined from fluctuations, deviation from the thermodynamical scaling might happen even for the SC model, when the non-equilibrium relaxation is concerned.

5.6.3 Relation between nucleation (toward the crystal branch) and non-equilibrium relation (toward the glass branch)

One may have a question if the non-equilibrium relaxation toward the crystal branch and that toward the glass branch is the same process or not. Therefore, relationship between nucleation (toward the crystallization) process and non-equilibrium relaxation is discussed here.

If one considered that the system relaxed toward the crystal branch, the phenomena investigated along the non-equilibrium relaxation might be considered as a rapid nucleation rather than the relaxation toward the glass branch. However, it was shown that the metastable structures on the glass branch are not FCC or mixtures of FCC and BCC crystals [10] but a mixture of their partial structures in an atomistic length scale. Therefore, during the non-equilibrium relaxation, structures tend to be locally (or in a medium ranged scale) equilibrated, while crystallization requires a nucleation and development of clusters and global rearrangements of positions of particles. Therefore, the non-equilibrated relaxation and the crystallization are not the same process, although some overlaps of processes are possible as already mentioned. Small difference of the structures obtained by different M values can be explained by the overlap of the partial crystallization or the changes in the local or medium packing caused by the fluctuation in the system.

5.6.4 Is the glass transition purely kinetic or with structural change?

In the present work, change of the packing of the system affected by the fluctuation of the thermodynamic quantities in the system was found. On the other hand, there is a claim that the glass transition is purely kinetic phenomena [For example, see discussion in Ref. 37]. That is, glass transition is considered to be brought by the short observation time compared with the relaxation time in this case. This view might be brought by the fact that the clear structural changes accompanied with the glass transition have not

been found in experiments. However, both experiments and simulations suggest the existence of structural change accompanied with the glass transition. Experimentally, it is known that the volumetric change of the systems occurs both at T_g and T_B with decreasing temperature (see Ref. 38 and references therein) and this fact implies that the location of free volumes in the system changes with temperature. Usually, aging of the glass is observed with volume change of the system [39] and therefore, such a “kinetic glass” will not be stable for a longer time scale. Therefore, existence of the kinetic glass is not necessarily contradicting to the existence of structural changes at these characteristic temperatures. MD simulations for several systems show sharpening of the first peak and/or splitting of the second peak of the pair correlation functions [6,40] and such splitting is accompanied with the structural arrest of the system [40]. Changes of the coordination polyhedra formed by oxygens around alkali metal ions were found during the glass transition in a silicate system [41]. Furthermore, structures of Voronoi polyhedra and their connections also change during the solidification of metallic glasses [42].

Structural changes near the characteristic temperatures are also known for an ionic liquid system. In the MD of EMIM-NO₃ [33], diffusion coefficient plotted against $1/T$ changes in slope at around T_B (~400 K), although it is difficult to reach the diffusive time regime near T_g by MD within a run of ~10 ns. Both a degree of freedom of geometrical structure of the coordination polyhedra of ions and a degree of freedom of the system measured by the number of fictive bonds (contact ion pairs) are found to change at these characteristic temperatures of ionic liquid [33]. Thus nowadays, many researchers of glass transition are seeking for the structural origin of the glass transitions

including theoretical ones (See Ref. 43 and references therein) and our MD simulations of the present simplest glass forming model is consistent to this view.

6. CONCLUSION

We have examined thermodynamic properties of the one component SC system and obtained analytical expressions of non-equilibrium relaxation under the constant pressure condition for the first time. Our main results are equations (11) and (16), where the non-equilibrium relaxation is represented by a time dependent term $j(\rho_t^*)$ (Instantaneous enthalpy H_t divided by $Nk_B T$). In Eq. (11), the value is represented as the function of both energy and number density. This is in contrast that the relaxation in *NVE* condition is a function of number density only. In equation (16), the $j_t^*(\rho^*)$ value is represented as a function of the compressibility factor, $g(\rho^*) (= \tilde{P}(T^*))$ and this enables us to compare the behavior of the systems using the phase-diagram represented by $g(\rho^*)$ against ρ^* plot. The contribution of internal energy term for the non-equilibrium relaxation is found to be about 1/4 of the instantaneous compressibility factor, $g(\rho_t^*)$. Validity of these expressions was confirmed by the molecular dynamics simulations with a suitable choice of mass of the wall used in the constant pressure conditions.

It was clarified that the plot of non-equilibrium relaxation in *NPH* condition mapped on the $g^* - \rho^*$ diagram is found to show a unique path with large fluctuations. The

fluctuation of the system brought by the different mass of walls was found to affect the packing of the particles in the system.

From these results, importance of the paths and fluctuations of the system on the phase-diagram for the discussion of the glass transition is suggested and they give a new perspective for understanding glass transition. Present work for constant pressure condition can be a basis to consider the relation between glass transition and fluctuations as well as its relation with extended conditions to affect it.

References

- [1] K.L. Ngai, *J. Non-Cryst. Solids*, **351**, 2635(2005).
- [2] C.A. Angell, *Nature*, **393**, 521 (1998).
- [3] C.A. Angell, *J. Phys.: Condens. Matter*, **12**, 6463 (2000).
- [4] P.W. Anderson, *Science*, **267**, 1616 (1995).
- [5] H.C. Andersen, *J. Chem. Phys.*, **72**, 2384 (1980).
- [6] Y. Hiwatari, H. Matsuda, T. Ogawa, N. Ogita and A. Ueda, *Prog. Theor. Phys.*, **52**, 1105 (1974).
- [7] M. Tanemura, Y. Hiwatari, H. Matsuda, T. Ogawa, N. Ogita and A. Ueda, *Prog. Theor. Phys.*, **58**, 1079 (1977); *ibid.*, **59**, 323 (1977).
- [8] M. Tanemura, H. Matsuda, T. Ogawa, N. Ogita and A. Ueda, *J. Non-Cryst. Solid* **117/118**, 883 (1990).
- [9] H. Ogura, H. Matsuda, T. Ogawa, N. Ogita and A. Ueda, *Prog. Theor. Phys.*, **58**, 419 (1977).
- [10] J. Habasaki and A. Ueda, *J. Chem. Phys.*, **134**, 084505 (2011).
- [11] J. Habasaki and A. Ueda, *J. Chem. Phys.*, **138**, 144503 (2013).

- [12] J.N. Cape and L.V. Woodcock, *J. Chem. Phys.*, **72**, 976 (1980).
- [13] S.L. Shumway, A.S. Clarke and H. Jónsson, *J. Chem. Phys.*, **102**, 1796 (1995).
- [14] W. Kob and H.C. Andersen, *Phys. Rev. E*, **51**, 4626 (1995); W. Kob, C. Donati, S.J. Plimpton, P.H. Poole and S.C. Glotzer, *Phys. Rev. Lett.*, **79**, 2827 (1997).
- [15] P. Bordat, F. Affouard, M. Descamps, and K.L. Ngai, *Phys. Rev. Lett.*, **93**, 105502 (2004); F. Affouard, M. Descamps, L.-C. Valdes, J. Habasaki, P. Bordat and K.L. Ngai, *J. Chem. Phys.*, **131**, 104510 (2009).
- [16] S.M. Stishov, *Soviet Phys. Usp.*, **17**, 627 (1975).
- [17] C. Dreyfus, A. Aouadi, J. Gapinski, M. Matos-Lopes, W. Steffen, A. Patkowski, and R.M. Pick, *Phys. Rev. E*, **68**, 011204 (2003).
- [18] R. Casalini, and C.M. Roland, *Phys. Rev. E*, **69**, 062501 (2004).
- [19] D. Coslovich and C.M. Roland, *J. Phys. Chem. B*, **112**, 1329 (2008).
- [20] K.L. Ngai, J. Habasaki, D. Prevosto, S. Capaccioli, and M. Paluch, *J. Chem. Phys.*, **137**, 034511(2012); **140**, 019901 (2014).
- [21] J. Habasaki and K.L. Ngai, *Phys. Chem. Chem. Phys.*, **9**, 4673 (2007).
- [22] K. Binder, *J. Non-Cryst. Solids*, **274**, 332 (2000).
- [23] J. Habasaki and K.L. Ngai, *J. Chem. Phys.*, **139**, 064503 (2013).
- [24] U.R. Pedersen, N.P. Bailey, T.B. Schröder, and J.C. Dyre, *Phys. Rev. Lett.*, **100**, 015701 (2008).
- [25] N.P. Bailey, U.R. Pedersen, N. Gnan, T.B. Schröder, and J.C. Dyre, *J. Chem. Phys.*, **129**, 184507 (2008).
- [26] S. Nosé, *Mol. Phys.*, **52**, 255 (1984); W. G. Hoover, *Phys. Rev. A*, **31**, 1695(1985).
- [27] J. Habasaki and A. Ueda, *Phys. Chem. Chem. Phys.*, **14**, 7120 (2012).

- [28] A. Ueda, *Molecular Simulations*, Shokabo, Tokyo (2003) in Japanese; A. Ueda, *Computer Simulation*, Asakura Shoten, Tokyo (1990) in Japanese.
- [29] R. Vautard, P. Yiou, and M. Ghil, *Physica D*, **58**, 95(1992); SSA is a principal component analysis of time series. We have found that 2-3 principal components are enough to represent the trend observed for the relaxation curves.
- [30] N.H. Packard, J.P. Crutchfield, J.D. Farmer and R.S. Shaw, *Phys. Rev. Lett.*, **45**, 712(1980).
- [31] J. Habasaki, K.L. Ngai and Y. Hiwatari, *J. Chem. Phys.*, **122**, 054507 (1-10) (2005).
- [32] J. Habasaki and K.L. Ngai, *J. Chem. Phys.*, **129**, 194501 (2008).
- [33] J. Habasaki and K.L. Ngai, *J. Chem. Phys.*, **142**, 164501 (2015).
- [34] W.G. Hoover and M. Ross, *Contemp. Phys.*, **12**, 339 (1971).
- [35] W.G. Hoover, S.G. Gray, and K.W. Johnson, *J. Chem. Phys.*, **55**, 1128 (1971).
- [36] J.L. Lebowitz, J.K. Percus and L. Verlet, *Phys. Rev.*, **153**, 250 (1967).
- [37] F.H. Stillinger and P.G. Debenedetti, *Annu. Rev. Condens. Matter Phys.*, **4**, 263 (2013).
- [38] K.L. Ngai and J. Habasaki, *J. Chem. Phys.*, **141**, 114502 (1-16) (2014).
- [39] H.R. Lillie, *J. Amer. Ceram. Soc.*, **16**, 619 (1933); N. M. Brandt, *J. Amer. Ceram. Soc.*, **34**, 332 (1951).
- [40] J. Habasaki and I. Okada, *Molec. Simul.*, **8**, 179 (1992).
- [41] J. Habasaki, *Molec. Phys.*, **70**, 513 (1990).
- [42] Y-F. Mo, R-S. Liu i, Y-C. Liang, H-T. Zhang, Z-A. Tian, Z-Y. Hou, H-R. Liu, L-L Zhou, P. Peng, T-H. Gao, *Comput. Mater. Sci.*, **98**, 1 (2015).

- [43] P. Ronhovde, S. Chakrabarty, D. Hu, M. Sahu, K.K. Sahu, K.F. Kelton, N.A. Mauro, and Z. Nussinov, *Eur. Phys. J. E***34**, 105 (2011).